Single-molecule tracking of myosins with genetically engineered amplifier domains

Christine Ruff[1], Marcus Furch[2], Bernhard Brenner[1], Dietmar J. Manstein[2] and Edgar Meyhöfer[1]

[1]Molecular and Cellular Physiology, Medical School Hanover, Carl-Neuberg-Str. 1, 30625 Hannover, Germany. [2]Department of Biophysics, Max-Planck-Institute for Medical Research, Jahnstr. 29, 69120 Heidelberg, Germany.

We combined protein engineering and single molecule measurements to directly record the step size of a series of myosin constructs with shortened and elongated artificial neck domains. Our results show that the step size has a clear linear dependence on the length of the neck domain and we also established that mechanical amplification in the myosin motor is based on a rotation of the neck domain relative to the actin-bound head. For all our constructs, including those with artificial necks, the magnitude of the neck rotation concurrent with the displacement step was ~30°. The engineered change in the step size of myosin marks a significant advance in our ability to selectively modify the functional properties of molecular motors.

Myosins are cellular motor molecules that use the energy derived from the hydrolysis of ATP to cyclically interact with and move along actin filaments. Myosin II is a heterohexamer consisting of two identical heavy chains and two pairs of essential and regulatory light chains. The N-terminal end of each heavy chain forms a large globular head that represents the motor domain of myosin, which includes the ATPase and actin binding sites. The rest of the heavy chains extend to form an 8.5 nm long α-helical neck region to which the light chains bind[1,2]. During each ATP hydrolysis cycle a myosin head binds to actin and generates one or several conformational changes with an overall displacement amplitude (step size) of 5 nm or larger[3–6].

Design of myosin motors with artificial necks

To analyze the functional role of the myosin neck we created eight motors with necks of different length (Fig. 1). We truncated *Dictyostelium* myosin at or near the junction between the converter domain[2] and the α-helical neck domain (either at residue Arg 761 or Ile 765) and fused the resulting head fragments to one or two α-actinin repeats. The shortest motor molecule, M765, contained no α-actinin repeat and was basically neckless, while the constructs with one and two α-actinin repeats (M765-1R, M761-2R, M765-1R, M765-2R) contained neck domains with predicted lengths of ~6 nm and 12 nm, respectively. Additionally, we used a construct (M864) similar to myosin subfragment 1 (S1) that contained the native light chain binding domains and associated light chains. To analyze the potential differences between single-headed and double-headed myosin, we compared the functional and kinetic properties of the single-headed constructs with two additional, double-headed motor molecules: enzymatically prepared heavy meromyosin (HMM) from rabbit skeletal muscle and an HMM-like *Dictyostelium* construct (HMM-2R) with two α-actinin segments in place of the light chain binding domains. Most constructs (Fig. 1) contained a His-tag at the C-terminus to facilitate purification and to allow specific attachment of the motor molecules *via* an antibody to the substrate.

Recording the step size

We determined the step size of our constructs with a custom-made microneedle-laser trap apparatus (Fig. 2) that is capable of detecting single acto-myosin interactions. Our measurements demonstrate that all constructs used in this study behaved similarly to vertebrate HMM and S1: at low surface densities of motor molecules and in the presence of ATP we identified transient events through the reduced Brownian fluctuations of the microneedle sensor, presumably resulting from binding of an immobilized myosin molecule to the actin filament (Fig. 3*a*,*b*). The step size of these events, which was obscured by large Brownian fluctuations, was determined using an analytical method similar to the one devised by Molloy and coworkers[3]. A single Gaussian distribution was fit to the histogram calculated from the mean position of a large number of transient acto-myosin interactions (Fig. 3*c*). In this analysis the shift in the

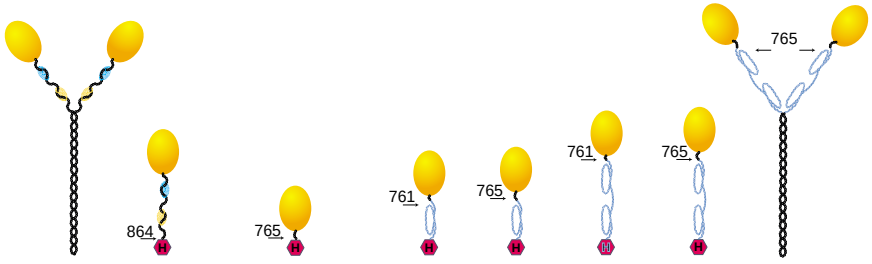

	HMM	M864	M765		M761-1R	M765-1R	M761-2R	M765-2R	HMM-2R
N	1195	635	993*	1735	414	1466	606	1413	790
M	6	6	4	5	3	5	5	4	6
neck length (nm)	7.5	7.5	0.6	0.6	6.0	6.6	12.0	12.6	12.6
step size (nm)	5.54±0.13	5.40±0.38	1.56±0.14	1.47±0.15	3.84±0.45	4.07±0.16	7.06±0.35	7.73±0.18	7.47±0.26

Fig. 1 Myosin molecules and step sizes. The diagram depicts in schematic form the organization of the different structural elements in the myosin molecules and constructs used in this study. The motor domains are shown as orange spheroids and the numbers next to the drawings indicate the residue at which the motor domain is truncated. The red pentagons mark the His-tags, and the α-actinin repeats are shown in dark blue. HMM-2R had an N-terminal His-tag (not shown) that was used for protein purification. Essential and regulatory light chains are shown as blue and yellow ellipses, respectively. The step sizes and estimated lengths of the neck domain for the different myosin motors are summarized in the lower part of the figure. N is the number of single acto-myosin events used to determine the step size. M is the number of filaments from which the events were pooled. The standard error of the step size was calculated from the fit of the Gaussian distribution to the histogram. For M765 we recorded the step size from antibody bound (indicated by a star) and directly adsorbed molecules.

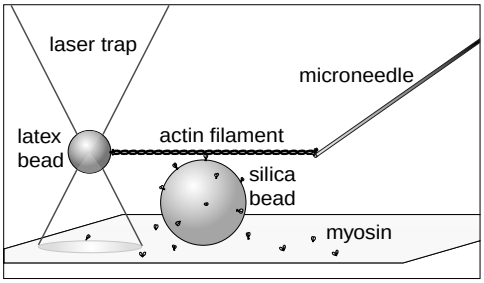

Fig. 2 Arrangement for recording single motor events. A single actin filament was attached to a microneedle and a trapped latex bead. The bead–actin filament–microneedle arrangement was assembled as described[3–5] and the actin filament was then carefully manipulated into the direct vicinity of a myosin coated silica bead to allow acto-myosin interactions. To reduce the compliance of the linkages from actin filament to microneedle and latex bead, the actin filament was pulled taut. The nitrocellulose surface coating of the silica bead and cover glass surface is not shown. For the step size measurements we used compliant microneedles (0.02–0.04 pN nm^{-1}) and a compliant laser trap (0.02 pN nm^{-1}) to minimally impede the power stroke of the motor.

mean position of the Gaussian distribution represents the amplitude of the step size.

Constructs with altered necks are competent motors

All the myosin constructs with altered neck domains investigated in this study were mechanically competent. They translocated actin filaments in multiple motor gliding assays and generated step displacements in single molecule experiments, irrespective of whether their neck was composed of an artificial α-actinin or the native light chain binding domain. Average *in vitro* gliding velocities for truncated constructs adsorbed directly to nitrocellulose coated surfaces were 124 ± 45, 107 ± 39, 169 ± 35, 170 ± 40 and 180 ± 39 nm s^{-1} for M864, M761-1R, M761-2R, M765-2R and HMM-2R, respectively. These velocities are in good agreement with previous reports[7]. Faster gliding velocities can be obtained when the proteins are adsorbed in a defined fashion *via* an antibody[7]. Event durations as a function of ATP concentration in the single-molecule experiments were consistent with an apparent second-order rate constant of ~2×10^6 M^{-1} s^{-1} for the ATP-induced dissociation of acto-myosin. Using established transient solution kinetics methods[7–9], we confirmed that the rate of this process was basically identical for all our constructs, with measurements ranging from 3–5×10^5 M^{-1} s^{-1}. The lower values determined using the system for measuring solution kinetics can be attributed to the high salt buffer conditions and the lower temperature used for these experiments. The step sizes, however, varied among the different constructs.

Myosin's step size is proportional to the neck length

Analysis of the mean position of the Gaussian event distributions for the different myosin motors revealed that the amplitude of the step size correlated with the length of the neck domain (Fig. 3*c*). Clearly, the Gaussian distributions for the construct with the shortest neck domain (M765) were centered near zero displacement, while those for the motors with the longest necks (M765-2R and HMM-2R) were shifted by a considerable distance. Also, the histograms consisting of large numbers of events are very well fit by a single Gaussian distribution (for example M765). This observation is consistent with the physical interpretation of the effect of the Brownian fluctuation of the actin filament and suggests that the residuals in the histograms are not due to a particular mechanism but simply represent expected statistical fluctuations. A regression analysis of our step size data revealed a linear relationship between the measured displacements and the estimated lengths of the neck domain (Fig. 3*d*). The step sizes of the myosin constructs with artificial neck domains and constructs with native neck domains were well fit by the same regression as indicated by an analysis of variance ($F \sim 708$, $P < 0.0001$) and the large correlation coefficient ($r^2 = 0.99$). Thus, myosin motors with an artificial α-actinin neck domain behaved, at least with respect to the generation of displacement, principally identically to those with wild type necks. For wild type myosin II, both from *Dictyostelium* and rabbit, we observed, in agreement with other studies[3,10,11], step sizes of just above 5 nm. Steps of 10 nm or more, or the larger steps of double-headed constructs[12] are not consistent with our observations.

We performed independent single-molecule experiments with M765 to test the influence of surface attachment and the directionality of movement. Recordings with polarity marked actin filaments established that M765, like myosin II, stepped towards the plus end of the actin filament. Also, the step size of M765 did not change when the molecules were bound either with an antibody or adsorbed directly to the surface (Fig. 3*d*). The observed 1.5 nm steps of M765 indicated that the pivot point of the lever arm cannot be located at the converter–neck junction, but must be located a few nanometers further inside the motor domain.

Myosin's neck rotates about a point near Gly 691

To determine if the observed step sizes can be explained quantitatively on the basis of a swinging lever arm model[1,7,13], we measured the length of the different neck domains using published crystallographic data (see summary in Fig. 1). We defined the converter–neck junction (Arg 761 in *Dictyostelium*) as the beginning of the neck domain. Thus, the neck of M765 consists of a 0.6 nm long, α-helical stretch. The length of the wild type neck of myosin was estimated from the distance to the beginning of a short α-helix (Trp 810) that runs approximately orthogonal to the neck domain and transmits forces and displacements to the C-terminal tail of myosin. In the chicken S1 structure[1] this segment (Lys 782–Trp 831) is ~7.5 nm long. The lengths of the α-actinin repeats were obtained from the crystal structure of M761-2R (ref. 14). In agreement with modeling[7,15,16] and structural observations[17], the functional lengths of one and two-repeat structures of α-actinin were 6 and 12 nm, respectively. The M761-2R crystal structure also showed that α-actinin domains emerge from the head in the proper orientation, with little angular deviation (<10°) relative to the native neck domain. Thus, our constructs with artificial necks were structurally intact motors. Using the linear relationship between displacement and lever arm length, extrapolation to zero step size places the origin of lever arm rotation (the hinge point) more than 2 nm inside the motor domain (Fig. 3*d*). Therefore, for all constructs used in this study, the functional length of the lever arm was 2.3 nm longer than the lengths of the neck domains, which reflects the distance from the hinge point to Arg 761. Our analysis, in agreement with structural work (reviewed in ref. 18), indicates that the hinge point of the lever arm is located near Gly 691 at the distal end of the SH1 helix.

Spectroscopic techniques have been applied to quantify the rotation of the myosin neck domain in muscle fiber preparations. For example, electron paramagnetic resonance data were interpreted as evidence for a 36 ± 5° rotation of the neck domain in scallop muscle fibers, but comparable changes could not be observed in rabbit muscle fibers[19]. In a different set of experiments, fluorescent probes were attached to the regulatory light

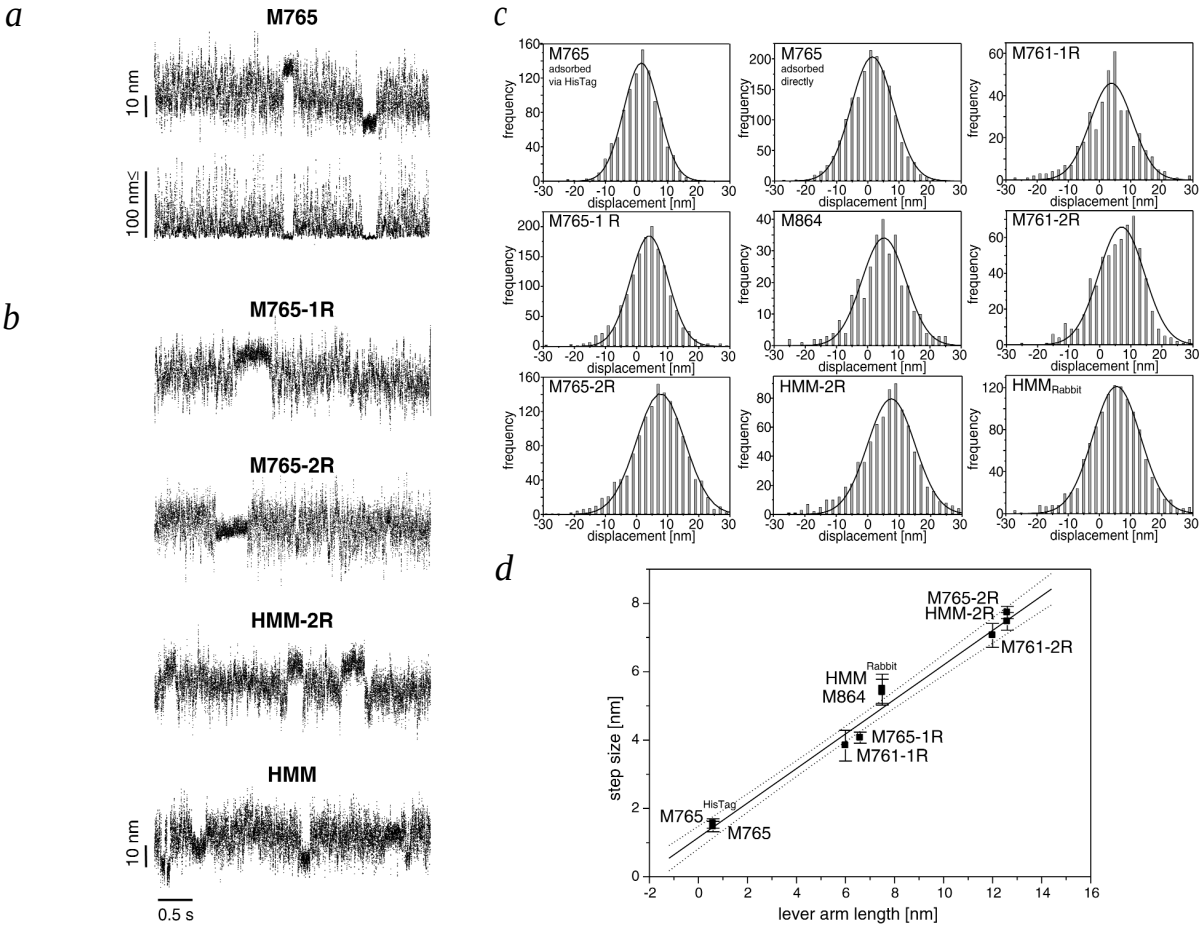

Fig. 3 Analysis of the step size behavior of myosin motors and constructs. ***a***, Raw displacement and running variance recordings. The tracing shows the interaction of an actin filament with the M765 construct. Displacement data (upper trace) were low-pass filtered at 1 kHz, and the length of the window for computing the running variance was 10 ms. In this short exemplary time series two single-molecule acto-myosin interactions are clearly visible. During the events the positional variance (lower trace) was reduced to below 5 nm^2. ***b***, Raw displacement recordings from myosin constructs with neck domains of different length. The displacement recordings from all myosin molecules used in this study appear basically identical: the Brownian fluctuations of the bead–actin filament–mircroneedle complex were transiently interrupted by single acto-myosin interactions. The large amplitude of the free fluctuations (~50–60 nm peak to peak) was determined by the combined stiffness of the laser trap and microneedle (0.04–0.06 pN nm^{-1}). Note the variable length of the events and the existence of events distributed over the entire range of positions sampled by the Brownian motion of the actin filament. ***c***, Frequency distribution of the events from different constructs. Histograms from all myosin molecules used in this study are shown. The shift in the fitted Gaussian distribution (solid lines) is interpreted as the step displacement generated by the myosin molecules. For the shortest construct with the smallest step size we independently confirmed the step direction with polarity marked actin filaments. The width of the Gaussian fits to the histograms (0.06 pN nm^{-1} for M765 with His-tag, 0.05 pN nm^{-1} for M765-1R, ~0.04 pN nm^{-1} for all others) confirmed the stiffness estimates obtained from calibrations of the free bead–actin filament–microneedle complexes just prior to recording and support our conclusion that events with a small step amplitude are superimposed on Brownian motion. In our assays the step size of myosin was attenuated by stretching the compliant connection from the actin filament to the microneedle. From the fluctuations during the events and the calibrated stiffness of the microneedle and laser trap we calculated that for all our measurements and constructs the step size was only ~4–6% larger than the observed displacement. The small differences in the stiffness of the microneedles have no influence on our analysis or any of our conclusions. ***d***, Regression analysis of the step size. The step sizes of the different myosin molecules were analyzed by a weighted linear model as a function of the lengths of the neck domains. The data from the M765 constructs adsorbed directly and *via* antibody were included separately. The dashed lines indicate the 95% confidence interval of the linear model.

chain and observed to rotate on average 2–3° upon changing the length of contracting muscle[20,21]. Based on the assumption that only a small fraction of the heads (~10%) responded to the imposed changes in length, it was concluded that this small fraction rotates through an angle of ~19° when the length of the muscle fibers was changed by a displacement corresponding to 3.6 nm per half sarcomere[20]. Using data from our single-molecule experiments, we directly calculated the angle of lever arm rotation. Assuming that the lever arm is straight and the plane of rotation is aligned with the actin filament axis, which on the whole is well justified by the crystal structure of myosin and the atomic model of the acto-S1 complex[1,22,23], we estimated the lever arm rotation during power strokes at low load to be ~30°.

By combining single-molecule functional analysis and genetic engineering we established that the light chain binding domain of myosin can be replaced with an artificial neck domain which serves to amplify small structural changes into displacement steps of several nanometers. This allowed us to selectively modify the mechanical gain and step size of the myosin motor. We recognize the potential of similarly modified motor proteins for nanotechnological or biotechnological uses. Now other key functional properties, such as processivity, direction of movement, and interaction with polymeric tracks need to be addressed to demonstrate that motor proteins are true contenders for such applications. Additionally, linking extended, rigid domains to molecular engines and

enzymes in general should facilitate single molecule recordings of conformational changes associated with transitions between states.

Methods

Construction, expression and purification of recombinant myosin molecules. Plasmids for the production of recombinant myosin motor domains were derived from the extrachromosomal vector pDXA-3H[24]. Expression vectors for the production of M765, M761-1R, M761-2R and M864 have been described[8,9,25]. Plasmids for the production of M765-1R and M765-2R contain the first 765 residues of the *Dictyostelium mhcA* gene fused to either residues 264–387 or residues 264–505 of the *Dictyostelium* α-actinin gene and a $(His)_8$-tag at their C-terminus. Plasmid pSA10 encoding HMM-2R was derived from pDH12-2R[7] by C-terminal fusion to codons 809–1224 of the *Dictyostelium mhcA* gene and N-terminal fusion to a sequence encoding a $(His)_7$-tag. Sequence analysis of the resulting constructs was carried out to confirm that the inserted fragment was unaltered and in-frame. *Dictyostelium* transformants were grown, selected, screened for the production of recombinant myosins, and protein was purified as described[26,27].

Combined microneedle/laser trap system. The set-up used for recording single acto-myosin interactions was similar to double laser trap systems[3–5] using the so-called three bead configuration, except that we replaced one of the trapped beads by a calibrated, fine microneedle with a stiffness typically ranging from 0.02–0.04 pN nm^{-1} and time constant of ~1 ms. The use of the microneedle has the advantage that rotation of the attached actin filament is reduced. The microneedle, in contrast to a trapped bead, is also stiffer in the directions orthogonal to the measurement axis. Details of microneedle systems have been described[27,28]. Briefly, we modified an inverted Zeiss Axiovert microscope with a piezoelectric stage (P730-20, Physik Instrumente), a high numerical aperture objective (Achroplan 100×, Zeiss) and custom-made dichroic mirrors to simultaneously observe rhodamine labeled actin filaments and beads, a brightfield image of the microneedle and beads, and to focus the beam of a near infrared diode laser (SK9648, Schäfter und Kirchhoff) for trapping. Steering of the laser trap was accomplished with a goniometer and the microneedle was held and manipulated with a piezoelectric three-axis positioner (M462, Newport). Microneedles were pulled from borosilicate glass[27]. A magnified brightfield image of the needle, projected onto a quadrant photo-diode (S1557, Hamamatsu), allowed position detection with subnanometer resolution and a bandwidth of >8 kHz. Signals were low-pass filtered (1 kHz), sampled at 5 kHz (AT-MIO-16E2, National Instruments) with a microcomputer and stored on disk for off-line analysis.

Single-molecule *in vitro* assays. All experiments were carried out at 23 ± 0.5 °C in 25 mM imidazole buffer at pH 7.4 with 25 mM KCl, 1 mM EGTA, 4 mM $MgCl_2$, 0.1–10 μM ATP, 10 mM dithiothreitol (DTT), 100 μg ml^{-1} glucose oxidase, 18 μg ml^{-1} catalase and 3 mg ml^{-1} glucose. Recording chambers (300 μl volume) were constructed from two cover glasses separated by a 1 mm thick teflon spacer such that a microneedle could be inserted from the side. First, the lower cover glass was coated with a 0.1% nitrocellulose solution (Fullam) in amyl acetate containing silica beads (Bangs) of 2.5 μm diameter as pedestals. Subsequently, we coated the surface with Penta-His antibody (Qiagen, 20 μg ml^{-1}) and attached His-tagged myosins (~0.1 μg ml^{-1}) by incubating for 10 min. Motor molecules without a C-terminal His-tag and HMM and HMM-2R were directly adsorbed to the nitrocellulose surface. For control measurements we also adsorbed a His-tagged construct (M765) directly to the nitrocellulose surface. Polarity marked actin filaments with a bright, fluorescent minus end were prepared by a method modified from Wells *et al.*[29]. Second order rate constants for the ATP induced dissociation of acto-myosin were estimated from event durations at different (0.1–10 μM) ATP concentrations.

Data analysis. To determine the step sizes of the different myosin constructs, we implemented a histogram based analysis method similar to the procedure first outlined by Molloy *et al.*[3] in a custom written C-program. Briefly, we computed a running estimate (10 ms time window) of the positional variance of the microneedle–actin–bead complex and identified individual events by the reduced fluctuation during binding to myosin. From the mean position of detected events we calculated a histogram. To obtain large data sets we pooled data from different actin filaments (Fig. 1). Only data from single filaments with a sufficiently large number of events that allowed an unequivocal determination of the orientation of the actin filament were incorporated into the final histogram. The number of individual myosin molecules contributing to each histogram was much larger than the number of actin filaments because, due to limited instrument stability, the actin filament drifted slowly from one myosin molecule to the next during long recording periods. Consistent with this behavior, we observed a temporal piling up of events during different portions of successful recordings. In addition, while recording with an individual actin filament we frequently changed to a different bead on the substrate. Fitting a Gaussian distribution (with mean and width as free parameters) to the histogram allowed us to estimate the shift of the distribution from the mean position and the uncertainty of the fit to the histogram.

Acknowledgments

We would like to acknowledge technical assistance from D.M. Hunt, U. Rühl, P. Uta and S. Zimmermann and help of the Zentrale Forschungswerkstätten with the construction of equipment. We thank M.L.W. Knetsch, S. Fujita-Becker and G. Tsiavaliaris for generous help. T.Q.P. Uyeda, S. Adlerstein, B. Sodeik, J. Kull and E. Ungewickell critically reviewed different versions of the manuscript and made many helpful suggestions. This work was supported by grants from the Deutsche Forschungsgemeinschaft (B.B., E.M.), Volkswagen-Stiftung (D.J.M., E.M.) and Max-Planck-Society (D.J.M.).

Correspondence should be addressed to E.M. *email: Meyhoefer.Edgar@MH-Hannover.de*

Received 8 June, 2000; accepted 1 December, 2000.

1. Rayment, I. *et al*. *Science* **261**, 50–58 (1993).
2. Houdusse, A. & Cohen, C. *Structure* **4**, 21–32 (1996).
3. Molloy, J.E., Burns, J.E., Kendrick-Jones, J., Tregear, R.T. & White, D.C.S. *Nature* **378**, 209–212 (1995).
4. Finer, J.T., Simmons, R.M. & Spudich, J.A. *Nature* **368**, 113–119 (1994).
5. Guilford, W.H. *et al. Biophys. J.* **72**,1006–1021 (1997).
6. Kitamura, K., Tokunaga, M., Iwane, A.H. & Yanagida, T. *Nature* **397**,129–134 (1999).
7. Anson, M., Geeves, M.A., Kurzawa, S.E. & Manstein, D.J. *EMBO J.* **15**, 6069–6074 (1996).
8. Kurzawa, S.E., Manstein, D.J. & Geeves, M.A. *Biochemistry* **36**, 317–323 (1997).
9. Ritchie, M.D., Geeves, M.A., Woodward, S.K.A. & Manstein, D.J. *Proc. Natl. Acad. Sci. USA* **90**, 8619–8623 (1993).
10. Veigel, C., Coluccio, L.M., Jontes, J.D., Sparrow, J.C., Milligan, R.A. & Molloy, J.E. *Nature* **398**, 530–533 (1999).
11. Mehta, A.D., Finer, J.T. & Spudich, J.A. *Proc. Natl. Acad. Sci. USA* **94**, 7927–7931 (1997).
12. Tyska, M.J. *et al. Proc. Natl. Acad. Sci. USA* **96**, 4402–4407 (1999).
13. Uyeda, T.Q.P., Abramson, P.D. & Spudich, J.A. *Proc. Natl. Acad. Sci. USA* **93**, 4459–4464 (1996).
14. Kliche, W. *et al. EMBO J.* **20**, 40–46 (2001).
15. Parry, D. A. D., Dixon, T.W. & Cohen, C. *Biophys. J.* **61**, 858–867 (1992).
16. Flood, G. *et al. J. Mol. Biol*. **252**, 227–234 (1995).
17. Djinovic-Caruga, K., Young, P., Gautel, M. & Saraste, M. *Cell* **98**, 537–546 (1999).
18. Geeves, M.A. & Holmes, K.C. *Annu. Rev. Biochem.* **68**, 687–728 (1999).
19. Baker, J.E., Brust-Mascher, I., Ramachandran, S., LaConte, L.E.W. & Thomas, D.D. *Proc. Natl. Acad. Sci. USA* **95**, 2944–2949 (1998).
20. Corrie, J.E.T. *et al. Nature* **400**, 425–430 (1999).
21. Hopkins, S.C., Sabido-David, C., Corrie, J.E.T., Irving, M. & Goldman, Y.E. *Biophys. J.* **74**, 3093–3110 (1998).
22. Dominguez, R., Freyzon, Y., Trybus, K.M. & Cohen, C. *Cell* **94**, 559–571 (1998).
23. Rayment, I. *et al. Science* **261**, 58–65 (1993).
24. Manstein, D.J., Schuster, H.-P., Morandini, P. & Hunt, D.M. *Gene* **162,** 129–134 (1995).
25. Furch, M., Geeves, M. A. & Manstein, D.J. *Biochemistry* **37**, 6317–6326 (1998).
26. Manstein, D.J. & Hunt, D.M. *J. Muscle Res. Cell Motil*. **16,** 325–332 (1995).
27. Meyhöfer, E. & Howard, J. *Proc. Natl. Acad. Sci. USA* **92,** 574–578 (1995).
28. Ishijima, A. *et al. Biophys. J.* **70,** 383–400 (1996).
29. Wells, A.L. *et al. Nature* **480,** 505–508 (1999).